Shock Waves (2016) 26:385–394
DOI 10.1007/s00193-015-0614-z

ORIGINAL ARTICLE

Shock wave emission during the collapse of cavitation bubbles

W. Garen[1] · F. Hegedűs[2] · Y. Kai[1,3] · S. Koch[1] · B. Meyerer[1] · W. Neu[1] · U. Teubner[1,3]

Received: 7 March 2014 / Revised: 4 December 2015 / Accepted: 10 December 2015 / Published online: 11 February 2016

Abstract Shock wave emission induced by intense laser pulses is investigated experimentally. The present work focuses on the conditions of shock wave emission in glycerine and distilled water during the first bubble collapse. Experimental investigations are carried out in liquids as a function of temperature and viscosity. Comparison is made with the theoretical work of Poritsky (Proc 1st US Natl Congress Appl Mech 813–821, 1952) and Brennen (Cavitation and bubble dynamics, Oxford University Press 1995). To the best knowledge of the authors, this is the first experimental verification of those theories.

Keywords Cavitation bubble · Laser-induced breakdown in liquids · Collapse shocks

Communicated by D. Ranjan.

This paper is based on work that was presented at the 29th International Symposium on Shock Waves, Madison, Wisconsin, USA, July 14–19, 2013.

✉ S. Koch
sandra.koch@hs-emden-leer.de

W. Garen
walter.garen@hs-emden-leer.de

[1] Institut für Laser und Optik, Hochschule Emden/Leer, University of Applied Sciences, Constantiaplatz 4, 26723 Emden, Germany

[2] Department of Hydrodynamic Systems, Budapest University of Technology and Economics, P.O. Box 91, 1521 Budapest, Hungary

[3] Institute of Physics, Carl von Ossietzky University of Oldenburg, 26111 Oldenburg, Germany

1 Introduction

The first investigations of the viscosity influence for the occurrence of an initial shock wave in liquids were carried out more than 50 years ago by Poritsky [1], Zababakhin [3], and 20 years ago by Brennen [2]. As a result, it was shown that the shock wave vanishes in liquids with a sufficiently high viscosity such as glycerine. Moreover, the numerical and experimental investigation of Hegedűs et al. [4] revealed that the formation of shock waves depends not only on the instantaneous Mach number, but also on the suitably defined instantaneous Reynolds number $Re = r(t)\dot{r}(t)/\nu$, where $r(t)$ is the time-dependent bubble radius and ν is the kinematic viscosity.

Due to the rapid decrease of the viscosity in liquids with increasing temperature, the viscosity influence is restricted to low temperatures for liquids. On the other hand, Brennen [2] found that the bubble and shock wave dynamics are mainly influenced by the vapor pressure if the temperature T_1 for the liquid is approximately 70–80 % of the boiling temperature T_b. In their study of laser-induced cavitation bubbles, Akhatov [5] suggested that a small amount of the non-condensable gas in a bubble may have a large influence on the bubble dynamics. The non-condensable gas in the bubble originates from plasma recombination phenomena and chemical reactions during the bubble development within a surrounding liquid. Lauterborn and Kurz [6] have investigated the bubble dimension applying a shadow method. In this present study, applying a purpose-built laser shadow method (LSM), a continuous measurement of the bubble dimension is possible and the exact timing of the emitted shock waves can be determined [8].

In this experimental setup, the spatial resolution is 0.01 mm, the temporal resolution is defined by the response time of the PIN diode which is 20 ns.

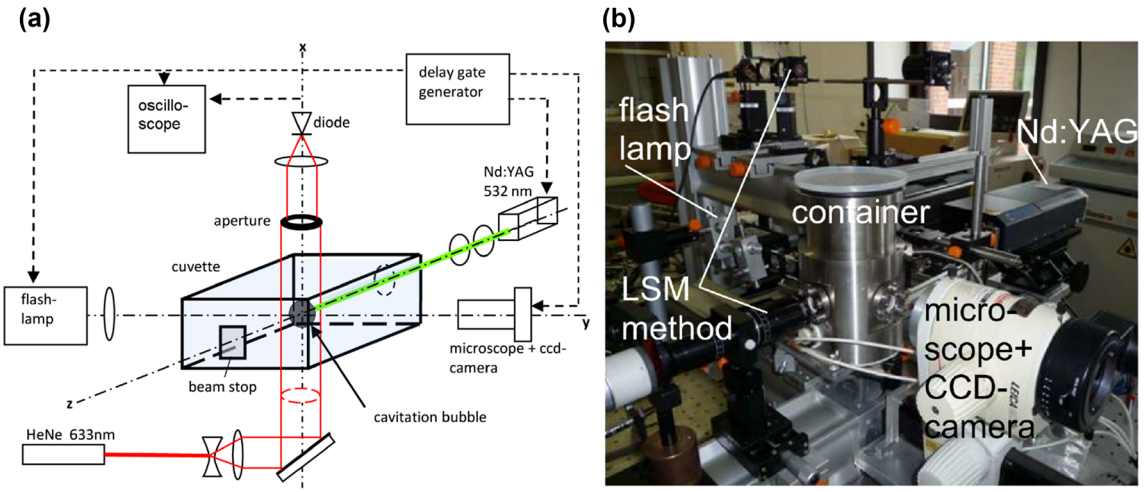

Fig. 1 Experimental setup. **a** sketch, **b** image

Lauterborn et al. [7] have investigated the influence of temperature on laser-induced bubbles. The present experiments have been extended to a great degree, so that the temperature and viscosity influence on the laser-induced bubbles, especially the collapse shock waves, are investigated systematically.

In real applications, such as the rapidly developing field of ultrasonic technology, the generated shock waves of a collapsing bubble can be used in many ways, e.g., to reduce the molecular weight of polymers [9], to increase the efficiency of heterogeneous catalysis [10] or to mix two immiscible liquids producing highly stable emulsions [11].

2 Experimental setup

Figure 1 illustrates the experimental setup. A Q-switched frequency-doubled Nd:YAG laser pulse (in z-direction) is focused into the middle of a 40 mm × 40 mm × 40 mm quartz cuvette (Fig. 1a) or in a steel container with controllable temperature and pressure (Fig. 1b), respectively. The laser parameters are: laser fluence 90 kJ/cm^2 (in focus), pulse duration 6 ns, wavelength 532 nm (Solo III PIV 15, New Wave Research). Bubble evolution is observed by a CCD camera (SensiCam, PCO, placed on a microscope). The shock wave after the optical breakdown, the expanding or shrinking bubble, the collapse shock waves and the bubble rebound can be displayed by the laser (HeNe) intensity modulation. The laser intensity modulation is measured by a PIN diode, thus it is proportional to the voltage modulation of the PIN diode (refer to Koch et al. [8] for a detailed description of the method).

A sketch of the detailed view of the measurement method can be seen in Fig. 2. The bubble has been centered in the middle of an expanded HeNe laser beam which has a Gaussian

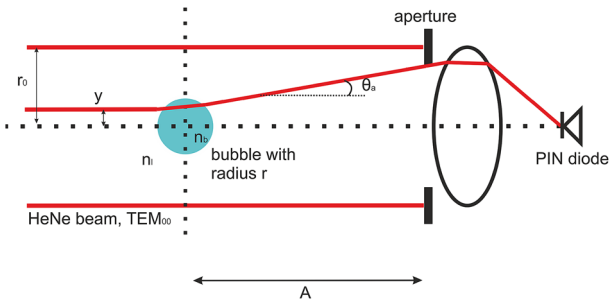

Fig. 2 Principle of the laser shadow method (LSM), detailed view

intensity distribution. Because of the smaller index of refraction of the bubble ($n \approx 1$), it acts like a diverging lens. The refraction angle is

$$\theta\left(n_\mathrm{b}, \frac{y}{r}\right) = \arcsin\left[\frac{n_\mathrm{l}}{n_\mathrm{b}} \cdot \frac{y}{r}\sqrt{1-\left(\frac{y}{r}\right)^2}\right] \tag{1}$$

n_l and n_b are the refractive indexes of the surrounding liquid and the bubble, respectively. y is the distance between the central axis (through bubble center) and the incident beam. r is the bubble radius. Most of the refracted beams penetrating the bubble will be blocked by the aperture. But at very small refraction angles $\theta < \theta_\mathrm{a}$, the beam can reach the diode (bubble light leakage), which leads to an error in the determination of the bubble volume. The limiting angle θ_a can be calculated from (1) as: $\theta_\mathrm{a} = (\frac{n_\mathrm{l}}{n_\mathrm{b}} - 1)\frac{y_\mathrm{a}}{r}$ if $(\frac{n_\mathrm{l}}{n_\mathrm{b}})^2(\frac{y}{r})^2 << 1$. Because $\theta_\mathrm{a} = \arctan(r_\mathrm{a}/A) \approx r_\mathrm{a}/A$ (refer to Fig. 2 and [8]),

$$\frac{y_\mathrm{a}}{r} = \frac{1}{A}\frac{1}{\frac{n_\mathrm{w}}{n} - 1} \tag{2}$$

In the current investigation: $A = 800$ mm, $r_\mathrm{a} = 0.5$ mm, $n_\mathrm{w} = 1.33$ and $n \approx 1$ which leads to $\frac{y_\mathrm{a}}{r} \approx 0.0038$. The error

depends inversely on the distance A. Since A is sufficiently large in this experiment, the error is very small, even for the case of a small bubble volume. However, right before the bubble collapses, n_b may increase rapidly because the vapor inside the bubble cannot condense fast enough, therefore $\frac{y_a}{r}$ from (2) increases. The time-dependent bubble radius ratio $r(t)/r_0 = z(t)$ can be calculated as a function of diode voltage ratio $U_d(t)/U_0 = u_d(t)$ in which r_0 is $1/e^2$ of the laser beam radius (Gaussian distribution) and the maximum diode voltage (without a bubble) is U_0.

$$z = \left\{ -\frac{1}{2} \ln[e^{-2z_a^2}(1 - u_d) + u_d] \right\}^{\frac{1}{2}} \tag{3}$$

When u_d approaches 1, z will approach 0. When u_d approaches 0, z will approach z_a with $z_a = \frac{r_a}{r_0}$.

3 Experimental results

3.1 Recorded signals

Figure 3 shows the evolution of the laser-induced bubble. The traces are obtained from the LSM-measurement. The images displayed with each graph are the corresponding shadow contours recorded with a CCD camera. This camera was illuminated by a flash provided by a 1 µs spark lamp or a separate 6 ns Nd:YAG laser, respectively, while a small fraction of the flash is also detected by LSM whose trace precisely indicates the point in time where the CCD image is taken. The advantage of the LSM-registration can be clearly seen in Fig. 3a. One measurement provides full information on the equivalent spherical bubble dimension, the exact position of the initial and the collapse shock waves as well as the (spherical) bubble dimension during the collapse and the rebound phase. CCD images in Fig. 3b–d show the bubble cross section (b) before, (c) during and (d) after bubble collapse, respectively. The cross sections (CCD images) are no longer spherical near the collapse phase. LSM automatically interprets the real bubble cross section as an equivalent spherical cross section which is without any influence on the exact time position of the collapse shock wave. The emitted shock wave is visible as a very sharp peak in the signal (Fig. 3a–d).

3.2 Dependence of the initial and collapse shock waves in glycerine on the temperature and pressure

In glycerine, experiments have been conducted in the temperature range from 20 to 110 °C (T_1 at constant pressure) and in the initial pressure range from 400 to 1050 mbar (P_1 at constant temperature). In Fig. 4, the results of different pressures or different temperatures are presented, respectively.

Collapse shock waves are only visible for $T_1 > (30–34\,°C)$, depending on initial conditions ($P_1 = 1$ bar, cf. Fig. 4b). It has been observed that a decrease of the initial pressure always leads to a prevention of collapse shock waves. In Fig. 4b, the liquid temperature has been changed from $T_1 = 30\,°C$ to $T_1 = 35\,°C$ ($P_1 = 1$ bar) and immediately a collapse shock wave appears which becomes even stronger with increasing temperature up to $T_1 = 110\,°C$, which is the highest temperature in the present investigation. It was observed that the initial shock waves generated by the laser-induced breakdown are always present under these pressure and temperature conditions.

3.3 Dependence of the collapse shocks in water on the initial temperature T_1

Due to the low viscosity values in distilled water, collapse shock waves are expected to occur. In particular, this is the case if $T_1 < 75\,°C$. Referring to Fig. 5a, the collapse shock waves become weaker, as the temperature increases from $T_1 = 24\,°C$ to $T_1 = 40\,°C$. For $T_1 \geq 75\,°C$, the bubble rebounds without a collapse shock. Furthermore, the collapse bubble radius increases with increasing T_1 (Fig. 5a). Figure 5b illustrates the details of the temporal position (see dotted arrow) between the LSM and the CCD image for capturing the shock wave and cavitation bubble.

3.4 Fit of the bubble distribution

To simplify further analysis, the experimental data of the bubble radius evolution has been fitted by a simple analytical relation.

$$r \cong r_{max} \cdot \left[\cos\left(\frac{\pi}{2} \cdot \frac{t}{t_2} \right) \right]^{\alpha} \tag{4}$$

with r_{max} the maximum bubble radius, $t_2 \approx t_{col}$ the collapse time, α is a fit parameter. t_2 is the theoretical time $t(r \rightarrow 0)$, which is approximately t_{col}. Because experimentally the bubble radius r is not 0 at the collapse, t_2 cannot be equal to t_{col}. The fitted curves in Fig. 6 agree very well with the experimental values. The bubble wall velocity and the wall acceleration (i.e., $\dot{r}$ and $\ddot{r}$) can be derived from (4) .

The experiments in water and in glycerine yield the following results for α (refer to Fig. 6 from $t = 0$ to $t = t_{col}$):

$\alpha < 0.4$ collapse shock waves occur;
$\alpha > 0.4$ no collapse shock waves present.

$\alpha = 0.4$ can be directly deduced from the Rayleigh–Plesset equation, when the effects of viscosity, non-condensable gas and surface tension are all neglected [12].

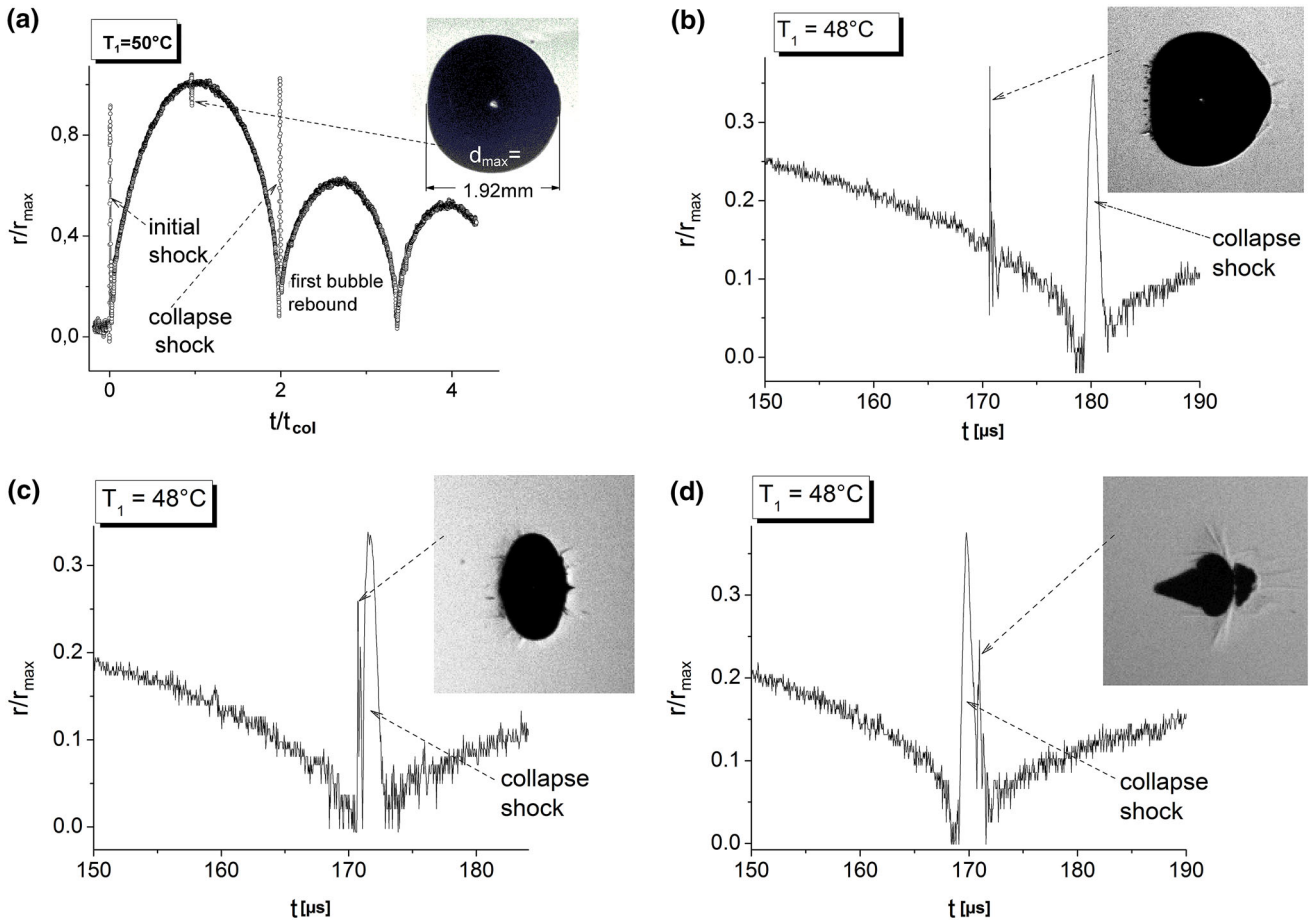

Fig. 3 LSM-measurements and shadow images in glycerine (dimensionless bubble radius normalized to maximum radius). The corresponding images are taken **a** at the maximum bubble radius, **b** approximately 9 µs before bubble collapse, **c** approximately 0.5 µs before bubble collapse, **d** approximately 1.2 µs after bubble collapse

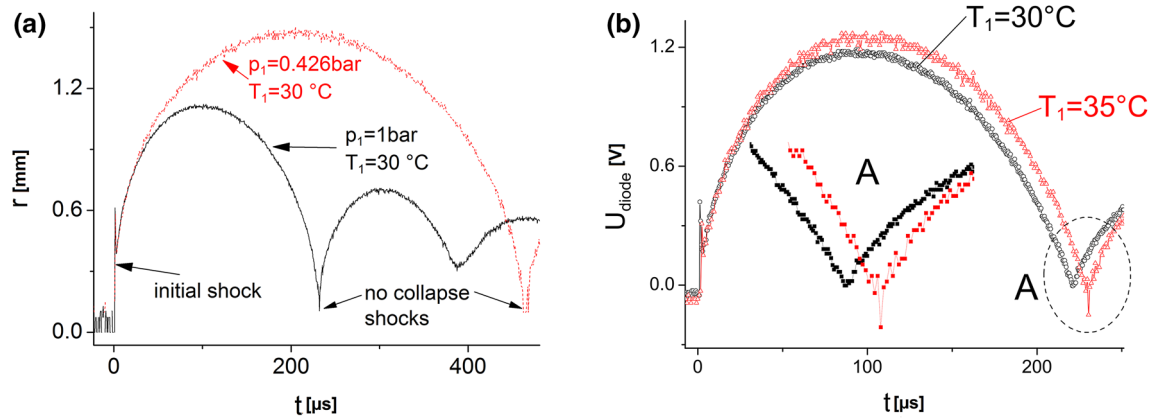

Fig. 4 LSM-measurements in glycerine, laser pulse energy ≅ 10 mJ. Results from **a** the pressure variation experiments, **b** the temperature variation experiments

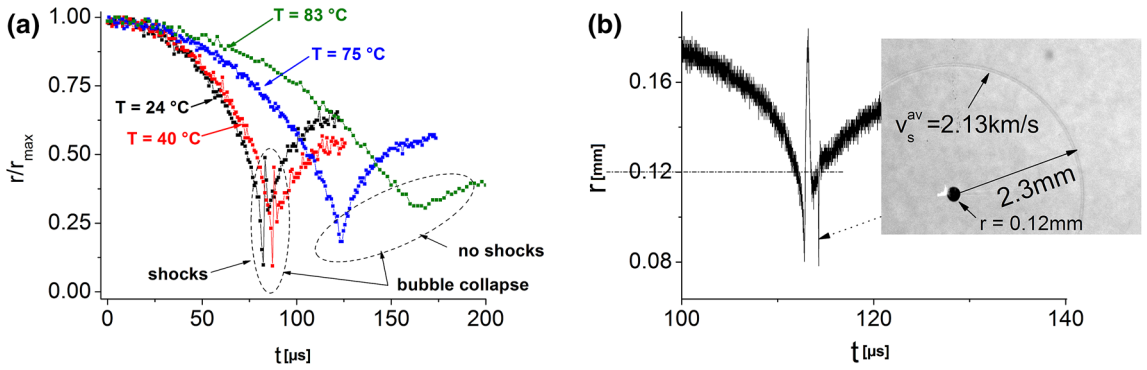

Fig. 5 Investigation of collapse shock waves in water: **a** time dependance of the bubble radius for different initial temperatures T_1, **b** details of the bubble radius as well as the temporal position of the shock wave and the bubble rebound. The sensitivity is increased by the reduction of aperture radius r_a

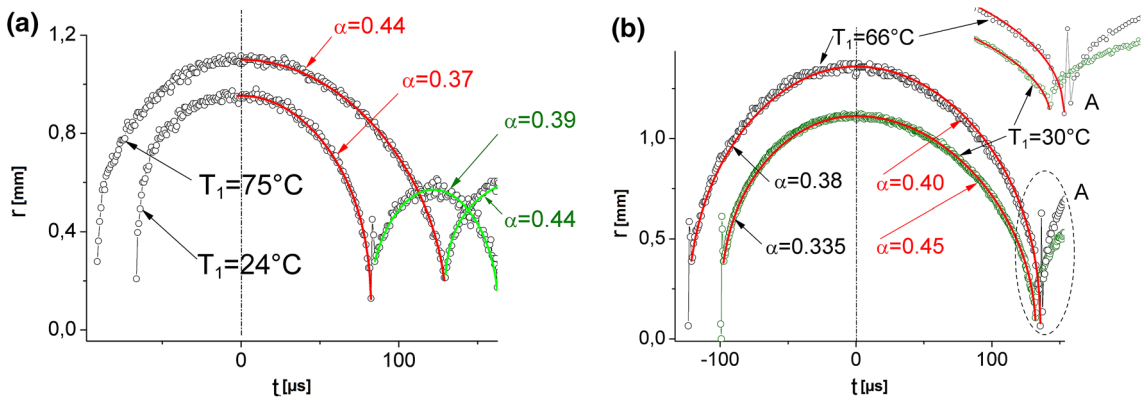

Fig. 6 Bubble radius r as a function of time t; experimental data and corresponding fits (*red curves*). **a** Water, **b** glycerine

Furthermore, assuming t is close to the collapse time t_{col}, one may deduce:

$$r \cong r_{\max} \cdot \left(\frac{t - t_{\mathrm{col}}}{t_{\mathrm{col}}} \right)^{\alpha} \tag{5}$$

In Fig. 7a the bubble wall velocities in distilled water ($T_1 = 75\,^{\circ}\mathrm{C}$) have been calculated as a function of the bubble radius r, whereas Fig. 7b shows similar results for glycerine ($T_1 = 30\,^{\circ}\mathrm{C}$). The plots of the velocity as a function of bubble radius show that the bubble trajectory consists of a shrinking loop. Furthermore, no gap in the shrinking loop is observed, which means there is no detectable collapse shock wave. Of course, this depends on the sensitivity of the LSM. Note that the LSM is able to detect a pressure wave as weak as $M_{\mathrm{s}} \approx 1.0002$, where M_{s} is the Mach number (refer to Appendix 1).

Figure 8a shows the smoothed curve of bubble radius as a function of time (each displayed data point is an average of 6 individual measurements under the same conditions; this is highly reproducible). Figure 8a has an average error of 6 % for $r_{\max}$ and up to 20 % for $r_{\min}$. The black curve in Fig. 8b is the first derivative of Fig. 8a, while the smooth red curve is obtained from all individual measurement points (in contrast to the black curve where the derivative is calculated from the averaged data points in Fig. 8a, for the red curve all individual data points are taken into account for the calculation of the derivative, which is subsequently averaged over 20 data points; this leads to a much smoother result). In Fig. 8c the smoothed velocity is plotted as a function of the bubble radius. In contrast to Fig. 7 ($T = 75\,^{\circ}\mathrm{C}$), Fig. 8 shows the experimental results for $T = 80\,^{\circ}\mathrm{C}$. Since $80\,^{\circ}\mathrm{C}$ is sufficiently higher than the limit of $75\,^{\circ}\mathrm{C}$ for water, it is ensured that no shock wave appears.

4 Theoretical interpretation

From the present measurements, the behavior of collapse shock waves in liquids can be summarized as follows:

1. *Lower temperature range* For liquids with high viscosity and low vapor pressure such as glycerine, the bubble

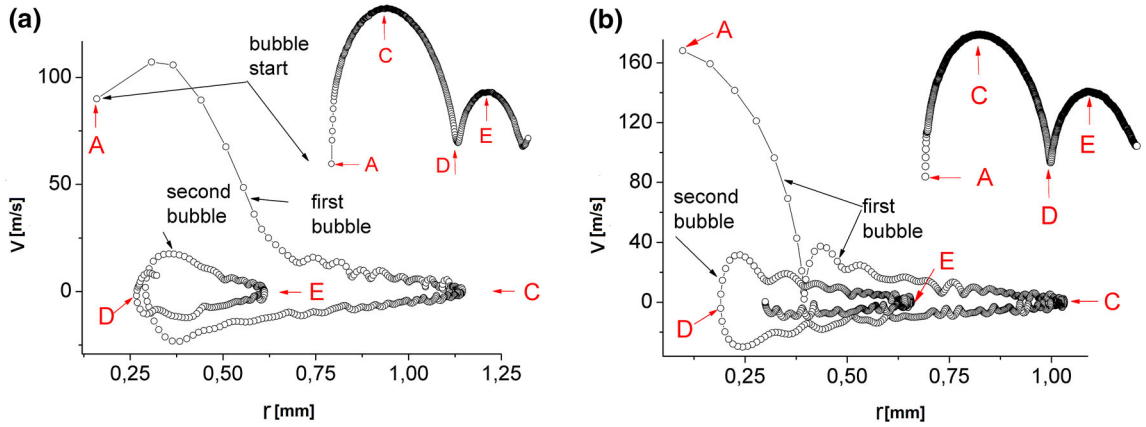

Fig. 7 Bubble wall velocity as a function of bubble radius. **a** Water, $T_1 = 75°C$, **b** glycerine, $T_1 = 30°C$

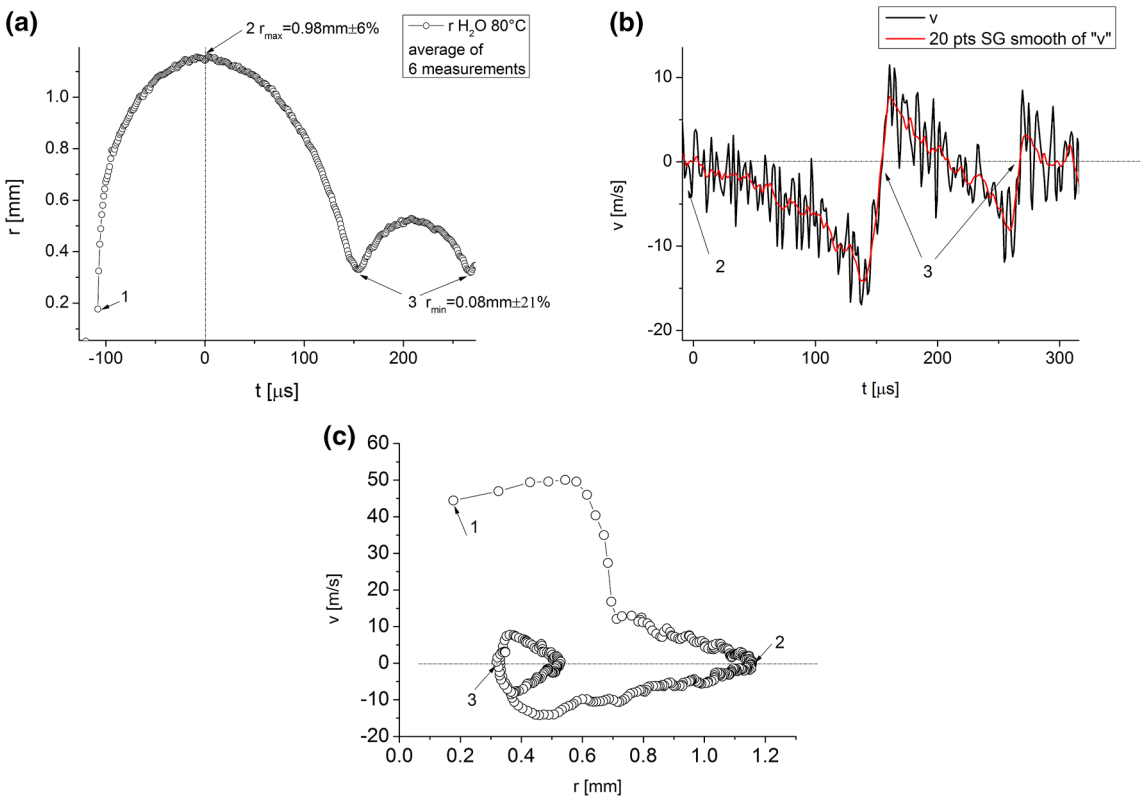

Fig. 8 Cavitation bubble development in water at 80 °C: **a** bubble radius as a function of time, **b** bubble wall velocity as a function of time, **c** bubble wall velocity as a function of radius

rebounds in the collapse phase without an emitted shock wave.

2. *Higher temperature range* When the vapor temperature approaches the boiling temperature, bubble rebound takes place without an emitted shock wave.

Consequently, the key parameters for a collapse shock to occur are the liquid viscosity and the liquid vapor pressure, both of which strongly depend on the temperature T_1.

Two temperature regions seem to be well-defined.

1. The lower temperature range was theoretically investigated by Poritsky [1]. He introduced the dimensionless number:

$$\mu^* = \frac{4\mu}{r_{\max}\sqrt{\epsilon\frac{p_1 - p_{v1}}{\rho_1}}}, \tag{6}$$

where μ is kinematic viscosity, $r_{\max}$ is maximum bubble radius, ϵ is 1 for a bubble collapse, ϵ is -1 for a bubble expansion. Both bubble expansion and collapse are slowed down by viscosity. Poritsky [1] found that if μ^*

is larger than approximately 0.46, the collapse time tends to be infinitely long.

In the present investigation, the lowest temperature T_1 investigated for glycerine was 30 °C which results in a dimensionless number of $\mu^* \approx 0.21$. This is a critical number μ^*_{cr} for the existence of collapse shock waves with the following relevance: If $\mu^* > \mu^*_{cr}$, collapse shock waves are present. But if $\mu^* < \mu^*_{cr}$, no collapse shock wave occurs.

Although this criterion has been proven for glycerine only, it is expected to be valid for other liquids with a sufficiently high viscosity. Otherwise for a low viscosity liquid such as distilled water, the critical value μ^*_{cr} cannot be reached. Moreover, the dimensionless number μ^* can also be used as a criterion for the existence of collapse shock waves in the higher temperature range. In Fig. 9a the curves have a minimum value at $T_1 \approx 78$ °C (water) and $T_1 \approx 249$ °C (glycerine). Again, the temperature T_1 that corresponds to the minimum of μ^* for water agrees very well with the experiments where the collapse shock waves (in water) disappear (Fig. 5a).

2. The results for the higher temperature range can be interpreted with the help of the calculations by Brennen [2] who analyzed thermal effects by introducing the parameter $\Sigma = \frac{(p_v \cdot L)^2}{\rho_l^2 \cdot c_{pl} \sqrt{\alpha_l}}$ as well as a "critical time" $t_{cr} = \frac{p_1 \left(1 - \frac{p_v}{p_1}\right)}{\rho_l \Sigma^2}$ (L is the latent heat of evaporation, c_{pl} is heat capacity of the liquid, and α_l is liquid thermal diffusivity).

In Fig. 10a the "thermodynamic parameter" Σ has been calculated for water and glycerine and Fig. 10b shows the "critical time" t_{cr} which is normalized to the bubble collapse time t_{col}. Both Σ and t_{cr} depend only on temperature and change by several orders of magnitude. For water the theoretical time ratio becomes $t_{cr}/t_{col} \approx 1$ for a temperature of $T_1 \approx 60$–80 °C. Our experiments in water show the same temperature range $T_1 \approx 75$ °C, where the collapse shock waves disappear.

For glycerine the appropriate temperature T_1 should be around 250 °C (Fig. 10b), which could not be proven experimentally since the liquid of glycerine becomes unstable.

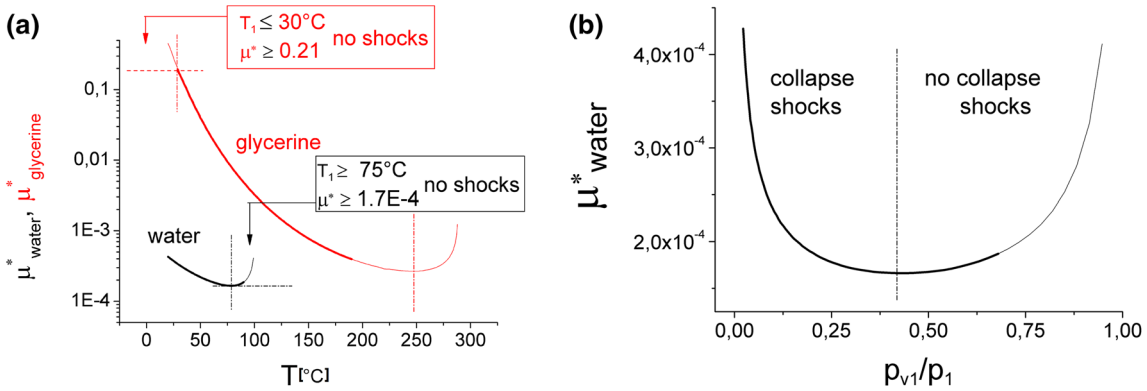

Fig. 9 **a** Dimensionless number μ^* as a function of temperature T_1. **b** μ^*_{water} as a function of the vapor pressure ratio. *Thicker lines* represent the experimental range

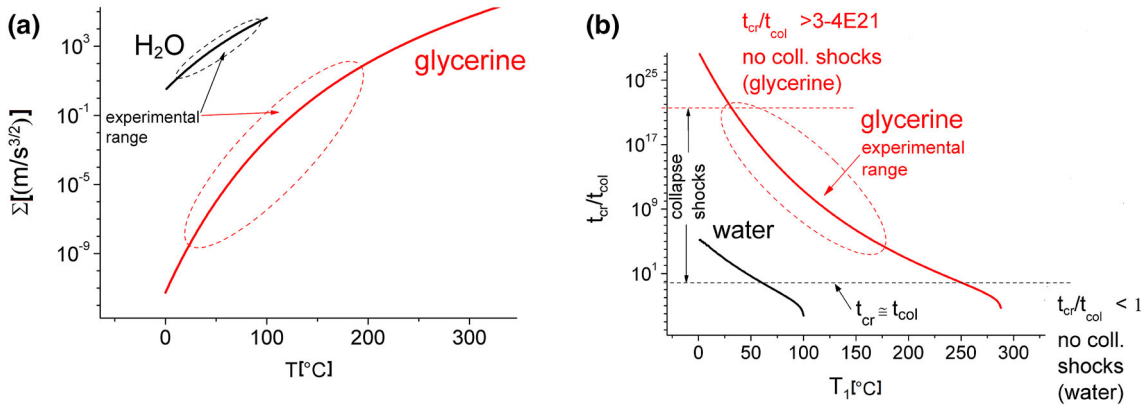

Fig. 10 Thermodynamic parameter Σ: **a** ratio of critical time and collapse time, **b** for water and glycerine as a function of the initial temperature T_1

T_{1cr} corresponds to the minimum of μ^*. Or in other words, T_{1cr} indicates the point where $\frac{d\mu^*}{dT_1}$ equals 0.
In the higher temperature range, when T_1 is higher than T_{1cr}, there is no collapse shock.
Figure 9b shows that μ^*_{water} depends on the vapor pressure ratio. The minimum value also corresponds to $T_1 \approx 78\,^\circ$C.
It is expected that both criteria, which have been proven independently in glycerine (first criterion) and water (second criterion), should be valid for other liquids as well. Further investigations on liquids of different viscosities will be carried out in the future.

5 Conclusion

Within the present experiments, the conditions for the occurrence of collapse shock waves with a laser-induced bubble have been investigated experimentally. The results can be summarized as follows:

1. For glycerine, a liquid with a high viscosity (at low temperatures), it tends toward a rebound without emitting a shock wave if the liquid temperature is less than 30 °C. For higher temperatures $T_1 > 35\,^\circ$C, the viscosity decreases rapidly and collapse shocks are present. This is consistent with the theory of Poritsky [1].
2. For water, at higher temperature, where the vapor pressure of the liquid becomes important, the bubble rebound takes place without a collapse shock. This has been demonstrated in distilled water.

Acknowledgments The authors would like to acknowledge support by the German National Science foundation (DFG; GA 249/9-1 and TE 190/8-1, Garen and Teubner), a grant from National Scientific Research Fund (OTKA), Hungary, project No: K81621 and the János Bolyai Research Scholarship of the Hungarian Academy of Sciences (Hegedűs).

Appendix 1: Estimation of the sensitivity of the LSM

From Fig. 11 the refraction angle ϵ can be calculated as:

$$\sin(\epsilon) = \frac{1}{1+\frac{\Delta n}{n_w}} \frac{y}{R} \sqrt{\left(1+\frac{\Delta n}{n_w}\right)^2 - \left(\frac{y}{R}\right)^2} \tag{7}$$

When $\frac{y}{R} = 1$ there is the maximum refraction angle ϵ_{max}.

$$\sin(\epsilon) = \frac{1}{1+\frac{\Delta n}{n_w}} \sqrt{\left(1+\frac{\Delta n}{n_w}\right)^2 - 1} \approx \epsilon_{max} \tag{8}$$

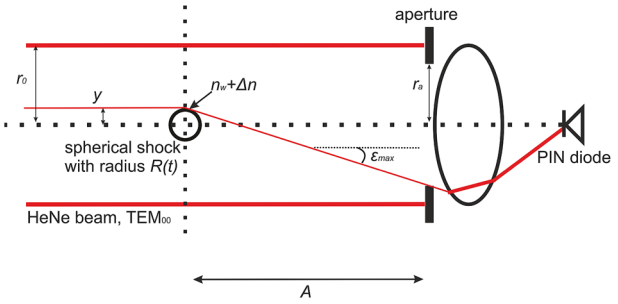

Fig. 11 Refraction of the incident beam by a spherical shock wave in water. The index of refraction for water is $n_w = 1.33$; the index of refraction behind the shock wave is $n_w + \Delta n(t) = n_s(t, M_s)$

If $\epsilon_{max} \geq r_a/A$ (acceptance angle of the diode, refer to Fig. 11), the illumination of the diode will be affected by the shock wave refraction.

For water, the sensitivity (in terms of the weakest detectable pressure wave) of the experimental setup in Fig. 11 can be determined by solving the Lorentz–Lorenz equation (9), a lithotripter equation (10) and the Tait equation (11).

The Lorentz–Lorenz equation is

$$\frac{n^2-1}{n^2-2} = K(\lambda)\rho, \tag{9}$$

where $K(\lambda) = \frac{n_0^2-1}{n_0^2-2}\frac{1}{\rho_0}$.

An equation obtained by the shock wave physics of lithotripters [12] is

$$M_s^2 = \frac{r}{n}\frac{r^n-1}{r-1}, \tag{10}$$

where $r = \frac{\rho}{\rho_0} = 1 + \frac{\Delta\rho}{\rho_0}$.

The Tait equation is

$$P = B\left[\left(\frac{\rho}{\rho_0}\right)^n - 1\right], \tag{11}$$

where P is the pressure. B and n are constants. $B_{water} = 3000$ bar and $n_{water} = 7.15$ (it is not the index of refraction!).

Thus, the sensitivity of the measuring arrangement can be estimated:

$$\left.\frac{\Delta\rho_w}{\rho_w}\right|_{min} \approx 3.7\left[\frac{1}{\sqrt{1-\left(\frac{r_a}{A}\right)^2}} - 1\right] \tag{12}$$

and

$$M_s^2 = \frac{1+\frac{\Delta\rho_w}{\rho_w}}{7.15}\frac{(1+\frac{\Delta\rho_w}{\rho_w})^{7.15}-1}{\frac{\Delta\rho_w}{\rho_w}} \tag{13}$$

With $r_a = 0.5$ mm and $A = 500$ mm, one obtains $\frac{\Delta\rho_w}{\rho_w}_{\min} \approx 5.56 \times 10^{-6}$ and $M_s \approx 1.0002$

Appendix 2: Role of the non-condensable gases

In this appendix, we discuss the role of the non-condensable gases for collapsing bubbles. It should be mentioned that, our investigation is focused on extreme initial conditions.

In the case of water, a vapor-filled bubble with an initial radius of $R_1 = 1.12$ mm and an initial vapor pressure of $P_{v1} = 385$ mbar ($T_1 = 75\,^\circ$C) shrinks to a bubble with a minimal radius of 0.2 mm and "rebounds" with a closed loop into a new expanding bubble. Although the present measurement method is very sensitive to density gradients, no shock is detected (the bubble does not collapse , even though there might be a weak pressure wave which emits into the liquid). On the contrary, the experiments in water with an initial temperature $T_1 < 75\,^\circ$C always show a weak collapse shock wave.

From the experimental results [refer to Fig. 13 (left) and Fig. 12 (left)], dR/dt and d^2R/dt^2 were calculated and the bubble pressures $P(t)$ were obtained by applying the Rayleigh–Plesset equation (14):

$$P(t) - P_1 = \rho_1 \left[R\ddot{R} + \frac{3}{2}\dot{R}^2 \right] + \frac{2\sigma}{R} + 4\eta\frac{\dot{R}}{R} \tag{14}$$

with surface tension σ, viscosity η, liquid density ρ_1 and ambient pressure P_1. This yields a maximum bubble pressure $P_{max} \approx 125$ bars for glycerine (Fig. 12, right) and $P_{max} \approx 113$ bars for water (Fig. 13, right). Assuming that a non-condensable gas (mainly air) results in P_{max}, the corresponding initial pressure $P(0)$ can be calculated for glycerine and water, respectively.

1. For glycerine: The non-condensated water vapor and air are responsible for the deceleration of the bubble wall during the (shock wave free) rebound without the bubble-collapsing. Since the water vapor pressure at 30 °C is negligibly small ($P(0)_{vap} < 1$ mbar), non-condensated air must be present. The initial gas pressure $P(0)_{gas}$ inside the bubble (assuming an adiabatic process), as the bubble shrinks from R_0 to R_{min}, can be calculated by the following equation:

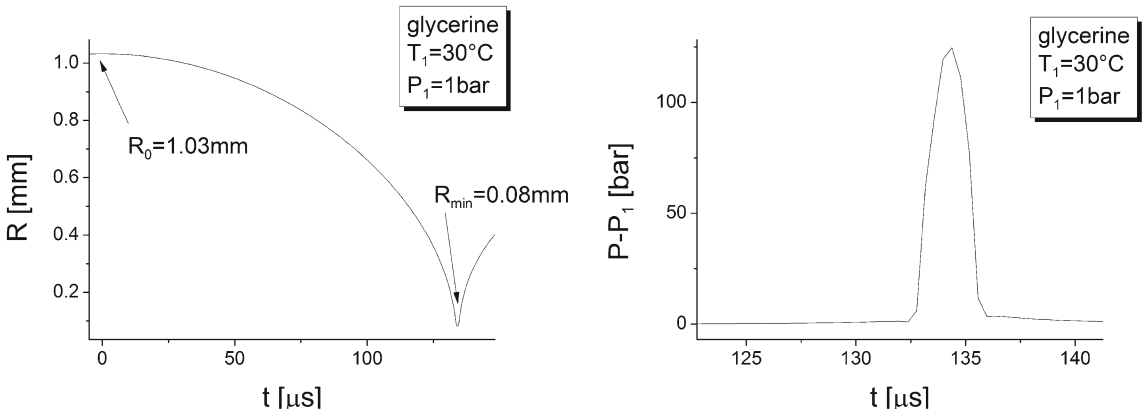

Fig. 12 Temporal development of the bubble radius R (*left*) and the pressure $P(t) - P_1$ (*right*), for glycerine

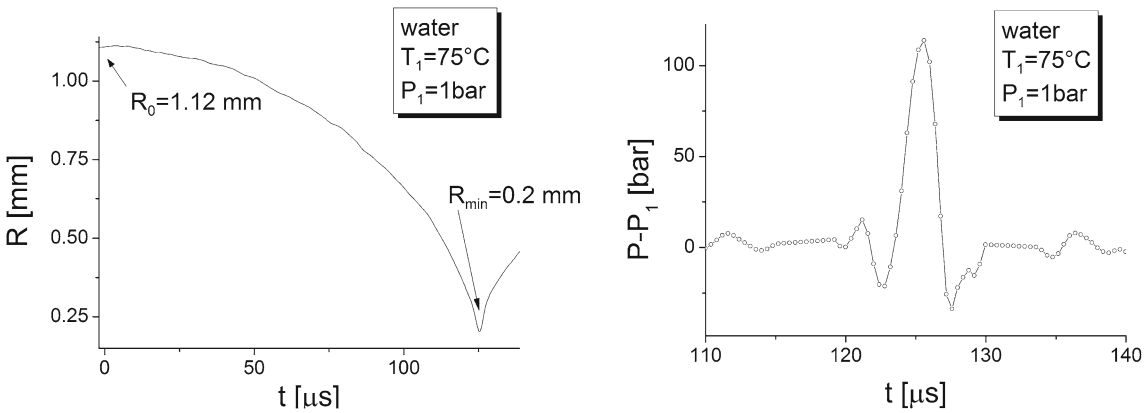

Fig. 13 Temporal development of the bubble radius R (*left*) and the pressure $P(t) - P_1$ (*right*), for water

$$P(0)_{\text{gas}} = P_{\max}\left(\frac{R_{\min}}{R_0}\right)^{3\gamma} \tag{15}$$

with the ratio of specific heat $\gamma = 1.4$, $R_{\min} = 0.08$ mm and $R_0 = 1.03$ mm. Thus $P(0)_{\text{gas}} \approx 2.7$ mbar. This is an acceptable value for the partial pressure of a non-condensable gas (mainly air) in glycerine at $T_1 \approx 30\,^{\circ}\text{C}$, whereupon this initial pressure might be the sum of partial pressures of air and water vapor because glycerine is hygroscopic.

2. For water: the situation is different from that of glycerine. At the initial temperature $T_1 \geq 75\,^{\circ}\text{C}$, there is a relatively high initial vapor pressure $P(0)_{\text{vap}} = 385$ mbar. However, the initial pressure of a non-condensable gas is low. If we assume a non-condensable gas (air and some small fraction of the non-condensated water vapor) stops the bubble wall at the minimum bubble radius, the required initial pressure can be calculated by the relation (15) with $R_{\min} = 0.2$ mm, $R_0 = 1.12$ mm. Thus $P(0)_{\text{gas}} \approx 81$ mbar.

The maximum partial initial pressure of air in water for $T_1 = 50\,^{\circ}\text{C}$ is $P(0)_{\text{air}} \approx 5.7$ mbar [13] and for $T_1 = 75\,^{\circ}\text{C}$ is even lower. It is comprehensible that the bubble shrinking is stopped by the remaining compressed water vapor inside the bubble which cannot condense fast enough before the bubble reaches the minimum volume [14,15]. The main reasons for this may be the increasing wall velocity and the decreasing bubble surface area which prevent the transport of the latent heat from the condensed vapor to the water surface.

References

1. Poritsky, H.: The collapse or growth of a spherical bubble or cavity in a viscous fluid. In: Proc. 1st US Nat. Congress of Appl. Mech, 813–821 (1952)
2. Brennen, C.E.: Cavitation and bubble dynamics. Oxford University Press, Oxford (1995)
3. Zababakhin, E.I.: The collapse of bubbles in a viscous liquid. PMM **24**(6), 1129–1131 (1960)
4. Hegedűs, F., Koch, S., Garen, W., Zoltán, P., Paál, G., Kullmann, L., Teubner, U.: The effect of high viscosity on compressible and incompressible Rayleigh-Plesset-type bubble models. Int. J. Heat Fluid Fl. **42**, 200–208 (2013)
5. Akhatov, I., Lindau, O., Topolnikov, A., Mettin, R., Vakhitova, N., Lauterborn, W.: Collapse and rebound of a laser-induced cavitation bubble. Phys. Fluids **13**(10), 2805–2819 (2001)
6. Lauterborn, W., Kurz, T.: Physics of bubble oscillation. Rep. Prog. Phys. **73**, 106501 (2010)
7. Lauterborn, W., Eick, I., Philipp, A.: Approaching bubble dynamics with lasers, holography and computers, Bubble dynamics and Interface Phenomena. Kluwer Academic Publishers, The Netherlands (1994)
8. Koch, S., Garen, W., Hegedüs, F., Neu, W., Reuter, R., Teubner, U.: Time-resolved measurements of shock-induced cavitation bubbles in liquids. Appl. Phys. B **108**, 345–351 (2012)
9. Konaganti, V.K., Madras, G.: Ultrasonic degradation of poly(methyl methacrylateco-alkyl acrylate) copolymers. Ultrason. Sonochem. **17**(2), 403–408 (2010)
10. Disselkamp, R.S., Judd, K.M., Hart, T.R., Peden, C.H.F., Posakony, G.J., Bond, L.J.: A comparison between conventional and ultrasound-mediated heterogeneous catalysis: hydrogenation of 3-buten-1-ol aqueous solutions. J. Catal. **221**(2), 347–353 (2004)
11. Freitas, S., Hielscher, G., Merkle, H.P., Gander, B.: Continuous contact- and contamination free ultrasonic emulsification—a useful tool for pharmaceutical development and production. Ultrason. Sonochem. **13**(1), 76–85 (2006)
12. Franc, J.P., Michel, J.M.: Fundamentals of Cavitation. Springer, Dordrecht (2004)
13. Harvey, A.H., Kaplan, S.G., Burnett, J.H.: Effect of Dissolved Air on the Density and Refractive Index of Water. Int. J. Thermophys. **26**(5), (2005)
14. Fujikawa, S., Akamatsu, T.: Effects of the non-equilibrium condensation of vapour on the pressure wave produced by the collapse of a bubble in a liquid. J. Fluid Mech. **97**, 481–522 (1980)
15. Fujikawa, S., Akamatsu, T.: Pressure waves radiated from bubbles collapsing with phase change, Shock Tubes and Waves. In: Proc. 12th Int. symposium on shock tubes and waves, Jerusalem, 169–179 (1979)